International Forum on Aeroelasticity and Structural Dynamics
IFASD 2019
9-13 June 2019, Savannah, Georgia, USA

GEOMETRICALLY NONLINEAR AEROELASTIC ANALYSIS WITH UNSTEADY VORTEX-LATTICE METHOD AND CFD

Natsuki Tsushima[1], Hitoshi Arizono[1], Masato Tamayama[1], Tomohiro Yokozeki[2], and Weihua Su[3]

[1] Japan Aerospace Exploration Agency
MItaka, Tokyo Japan
tsushima.natsuki@jaxa.jp
arizono.hitoshi@jaxa.jp
tamayama.masato@jaxa.jp

[2] The University of Tokyo
Hongo, Tokyo Japan
yokozeki@aastr.t.u-tokyo.ac.jp

[3] The University of Alabama
Tuscaloosa, Alabama USA
suw@eng.ua.edu

Keywords: aeroelasticity, structural analysis, multi-fidelity analysis, aircraft.

Abstract: In this paper, a comprehensive multi-fidelity aeroelastic framework for highly flexible wings is presented, which involves aerodynamic models with different fidelities. A corotational approach with shell finite elements is used to model the geometrical nonlinearity of flexible wings. An unsteady vortex-lattice aerodynamic method and a fast unstructured CFD code are coupled with the structural model subject to the large deformations, providing different fidelity solutions. The developed geometrically nonlinear aeroelastic solutions with different fidelities are compared to evaluate their accuracies and computational efficiencies.

1 INTRODUCTION

Wing morphing technique has recently been revisited due to the potential to improve aircraft performance and to facilitate economic flight. The morphing technique allows to adaptively change the wing shape in varying flight conditions and to achieve the optimal flight performance even in flight conditions in which conventional control surfaces compromise their performance. Consequently, the morphing technology may improve aerodynamic characteristics and reduce structural weight and acoustic noise of aircraft [1-4]. Additionally, it may enhance flight safety through improvement of stall characteristics and gust alleviation.
The performance of the morphing wing technology has been evaluated by many research groups in various projects. One of the contemporary concepts taking advantage of such wing morphing technique is the Variable Camber Continuous Trailing Edge Flap (VCCTEF) system [3]. Based on aerodynamic numerical simulations and wind tunnel tests, the VCCTEF system showed performance improvements in drag reduction and high-lift up to 6.31%.
A significant number of researches has been conducted on morphing wing technologies taking advantage of recent developments in structures and materials. For instance, Cooper et al. designed and evaluated a morphing wingtip for a regional jet advantageously using the

morphing concept and chiral-type auxetic structure [5]. Vasista et al. studied and tested a droop-nose morphing wing tip design with compliant structures as a part of European project NOVEMOR (Novel Air Vehicle Configurations: From Fluttering Wings to Morphing Flight) [6]. Smart materials such as piezoelectric materials were also considered to accomplish an effective wing morphing. Such piezoelectric-based morphing wings have the two advantages of fast response and high bandwidth. Morphing wings with piezoelectric materials could be used for suppressing aeroelastic instabilities and extending the flight envelope [7, 8]. In addition, the piezoelectric materials could also provide energy harvesting capability from wing vibrations by converting mechanical energies into electrical forms [9]. More recently, spanwise adaptive wings using shape memory alloy (SMA) actuators for Prototype-Technology Evaluation Research Aircraft (PTERA) was developed [10].

The active changes of wing geometry during flight may correspond to large deformations, but small strains, resulting in geometrically nonlinear deformations, limit-cycle oscillations (LCOs), and so on. Therefore, to accurately analyze morphing aircraft/wings for a better understanding of such wings, an aeroelastic model to consider the geometrical nonlinearities is important. Moreover, although the geometrical nonlinearity of highly flexible structures can be considered with nonlinear beam models [11, 12], nonlinear shell models are more suitable to study flexible wings involving finite deformations in the camber. The aerodynamic characteristics of such flexible wings can be evaluated by using computational fluid dynamics (CFD) [13-15]. However, the approach using CFDs is not effective in a preliminary development or a study with various wing designs since it compromises computational efficiency, especially in case the large wing motion is involved. As an alternative approach, an unsteady aerodynamic model with the panel methods can be coupled with a geometrically nonlinear finite element model for computational efficiency with adequately accurate solutions, which can be used for preliminary to middle stage of developments. Especially among different aerodynamic models used for problems subjected to the large deformations, an unsteady vortex-lattice method has shown to provide simplicity for implementation and computational cost reduction [16, 17].

In this paper, an integrated geometrically nonlinear, unsteady aeroelastic framework to analyze the nonlinear aeroelastic response of highly flexible wing have been developed. For structural model, a corotational approach with shell finite elements is used to consider the geometrical nonlinearity due to the large deformation of morphing wing. A UVLM formulation and a fast unstructured CFD code, which has been developed by JAXA[19], are coupled with the structural part. Numerical results with the integrated geometrically nonlinear, unsteady aeroelastic framework selecting different fidelity aerodynamic models are compared to evaluate in term of accuracies and computational costs.

2 MULTI-FIDELITY AEROELASTIC FRAMEWORK

2.1 Geometrically nonlinear structural analysis

By following the previous works [18, 19], the nonlinear structural dynamics of highly flexible wings is solved using three-node triangular shell element by a superposition of the optimal triangle membrane (OPT) and discrete Kirchhoff triangle (DKT) elements [20, 21] with a corotational approach [22]. The corotational shell finite element analysis solves translations and rotations of each node within the analysis frame as shown in Fig. 1. The analysis frame consists of the global frame G, the body frame B, the initial (undeformed) elemental frame E_0, and the current elemental frame E, respectively. Since the corotational approach can be utilized for large deformation problems independently of the choice of finite elements, if the approach is combined with simple but efficient finite elements, an effective geometrically

nonlinear analysis can be performed. A transformation matrix **T** of the initial orientation to the current orientation of each node in the current elemental frame *E* is given by

$$\mathbf{T} = \mathbf{T}_E^T \mathbf{T}_S \mathbf{T}_{E_0} \tag{1}$$

where $\mathbf{T}_E$ is the transformation matrix between the current elemental frame and the body frame, and $\mathbf{T}_S$ is the transformation matrix describing rotations of a nodal orientation. The nonlinear structural equations of motion is given by

$$\mathbf{Ma} + \mathbf{Cv} + \mathbf{K}(\mathbf{d}) = \mathbf{F} \tag{2}$$

where **M**, **C**, **K** are the global mass, damping (including the gyroscopic and stiffness proportional damping), and tangent stiffness matrices, which are assembled for the entire structures in the global frame, respectively. Also, **a**, **v**, **d** are the acceleration, velocity, and displacement vectors, respectively. The total force vector is denoted as **F**, which includes the external aerodynamic loads obtained by the UVLM or CFD. In the current work, the numerical integration of Eq. (2) is performed using the modified generalized-α method [23]. The detailed descriptions of the individual matrices can be found in Refs. [18, 19].

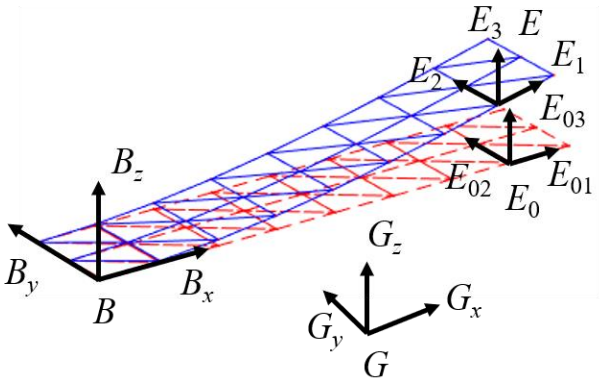

Figure 1: The structural analysis frame.

2.2 Aerodynamic analysis

To couple with the structural model subject to the large deformation, an unsteady vortex-lattice aerodynamic method (UVLM) [24] with the compressible correction [18] has been implemented for the medium fidelity analysis procedure. The UVLM can provide a cost-efficient aerodynamic solution considering wake flows. In the UVLM, the flow velocity can be solved by using the boundary condition, which is zero normal flow across the wing surface given by

$$\left(\nabla\Phi_B + \nabla\Phi_w + \mathbf{v}\right)\cdot\mathbf{n} = 0 \tag{3}$$

where **v** and **n** are the lifting surface velocity and the normal vector to the lifting surface, and Φ_B and Φ_w are the potential of the bound elements and shed wake. A detailed formulation of the UVLM and the coupling procedure for the structural analysis can be found in Refs. [18, 19]. For the high-fidelity analysis procedure, the fast CFD code "FaSTAR" developed by Japan Aerospace Exploration Agency (JAXA) [25] is coupled as the aerodynamic solver. Figure 2 shows the aerodynamic system frame *A* with the angle of attack α. The *x*-axis is

along the chord, while the *y*-axis is along the span. The unit normal vectors at a point on the upper and lower surfaces are denoted as $\mathbf{n^u}$ and $\mathbf{n^l}$. The mesh generation for the CFD is performed with the unstructured mesh generation code "MEGG3D" [26]. In the mesh generation, the same number of elements and nodes are generated for the upper and lower surface meshes to help the following transformation between the CFD and shell finite element. A CFD solution provides pressures and shear stresses due to frictions on the upper and lower surfaces.

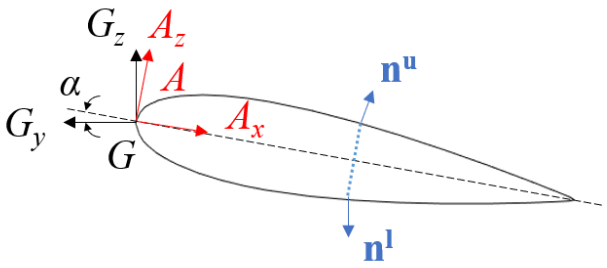

Figure 2: The aerodynamic analysis frame for the CFD.

2.3 Aero-structure interactions

In the medium-fidelity procedure, the aerodynamic mesh basically corresponds to the structural finite element mesh. On the other hand, in the high-fidelity procedure, the CFD mesh has considerably larger number of elements than the structural finite mesh. In addition, the aerodynamic pressures and friction coefficients obtained by the CFD are on the upper and lower surfaces of the wing, while the structural shell finite elements and corresponding nodes are on the surface crossing the wing camber line. Therefore, a transformation or projection is required to couple the aerodynamic outputs from the CFD with the structural shell finite element analysis. First, pressures and shear stresses at CFD grids on the upper and lower surfaces are projected onto the camber surface, which has the same number of grids as the two original surfaces as shown in Fig.3. Aerodynamic stresses on the camber surface in the aerodynamic frame can be calculated based on the projected loads from the grids on the upper and lower surfaces as

$$\mathbf{\Delta p_k} = p_k^l \cdot \mathbf{n_k^l} - p_k^u \cdot \mathbf{n_k^u} \tag{4}$$

$$C_k^{f_x} = q\left(c_{f_x,k}^l + c_{f_x,k}^u\right) \tag{5}$$

$$C_k^{f_z} = q\left(c_{f_z,k}^l + c_{f_z,k}^u\right) \tag{6}$$

where $\mathbf{\Delta p_k}$ is the pressure difference at the *k*th grid on the camber surface, p_k^l and p_k^u are the corresponding pressures on the original upper and lower surfaces, q is the dynamic pressure in the far field, $C_k^{f_x}$ and $C_k^{f_z}$ are the shear stresses due to the friction, $c_{f_x,k}^l$, $c_{f_x,k}^u$, $c_{f_z,k}^l$, and $c_{f_z,k}^u$ are the friction coefficients on the lower and upper surfaces in the A_x and A_z directions, respectively. In this study, only a component of $\mathbf{\Delta p_k}$ in the A_z direction, Δp_k^z, is considered for the pressure load. Next, based on the pressure and shear stress distributions on the projected shell surface, stress distributions on nodes of the shell finite elements as well as collocation points (center of elements) on each element can be calculated. Aerodynamic loads exerted on *m*th shell finite element in the aerodynamic frame are obtained from the stresses by multiplying the area of the *m*th shell element, s_m, as

$$Q_m^p = s_m \Delta p_m^z \tag{7}$$

$$Q_m^{f_x} = s_m C_m^{f_x} \tag{8}$$

$$Q_m^{f_z} = s_m C_m^{f_z} \tag{9}$$

where Q_m^p is the load due to the pressure, $Q_m^{f_x}$ and $Q_m^{f_z}$ are the loads due to the friction in the A_x and A_z directions, respectively. Finally, the lift and drag components of the aerodynamic loads in the structural frame on the mth element at the root angle of attach α can be obtained by the loads in the aerodynamic frame as

$$F_m^L = \left(Q_m^p + Q_m^{f_z}\right)\cos\alpha - Q_m^{f_x}\sin\alpha \tag{10}$$

$$F_m^D = -\left[\left(Q_m^p + Q_m^{f_z}\right)\sin\alpha + Q_m^{f_z}\cos\alpha\right] \tag{11}$$

A transformation from the aerodynamic loads on the collocation points to the structural grids on the shell finite elements is performed with the Thin Plate Spline (TPS) [18]. Figure 4 describes the algorithm of the high-fidelity aeroelastic analysis framework using the fast CFD code. The current high-fidelity analysis framework is not fully automated and requires manual data transfers between structural and aerodynamic solvers.

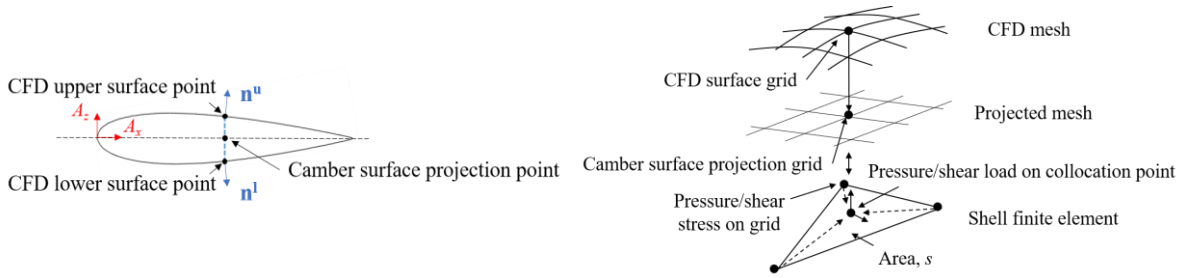

Figure 3: Interaction between the CFD grids and shell finite element information.

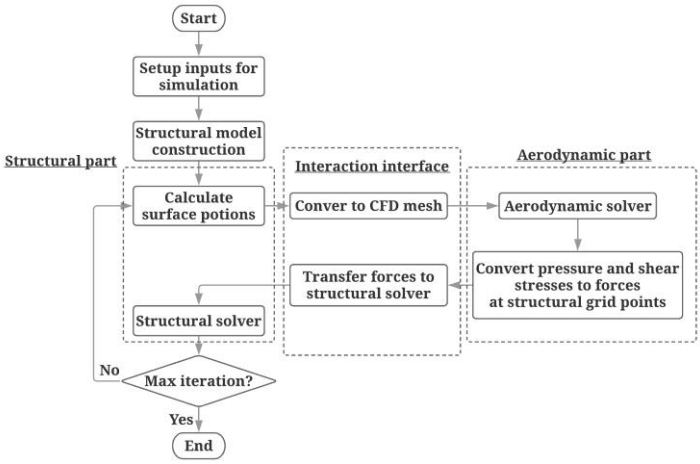

Figure 4: Algorithm of the high-fidelity aeroelastic analysis framework with the fast CFD.

3 NUMERICAL STUDIES

3.1 Analysis model

Figure 5 shows the rectangular thin wing model used in the study. The wing has the chord of 0.1 m and span of 1 m. The shell finite element model is discretized into 41 and 21 in the

chordwise and spanwise directions. The airfoil profile is NACA0010 and the wing is fixed at the root. The material properties of the flexible wing are Young's modulus E = 2.8 GPa and Poisson's ratio ν is 0.4. The flight condition is altitude h = 10,000 m, root angle of attack α = 5°, and Mach number M = 0.3. The CFD meshes are generated with approximately 55,000 elements.

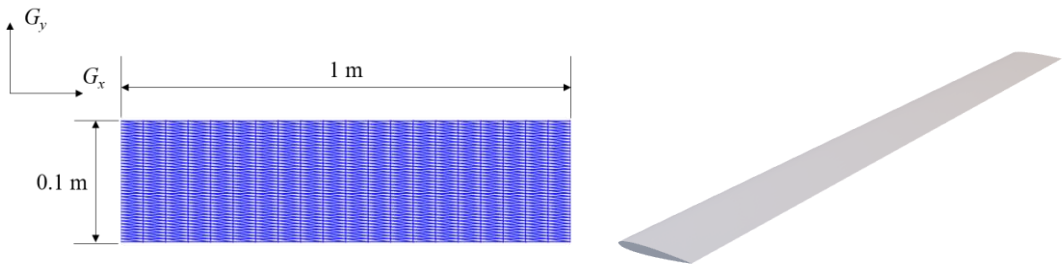

Figure 5: Planform and CFD model of the rectangular wing.

3.2 Multi-fidelity static aeroelastic analysis

To evaluate the performance difference in the medium-fidelity framework with the UVLM and the high-fidelity framework with the fast CFD code, comparisons of solutions are performed in this paper. In the high-fidelity analysis with the fast CFD code, the Euler equations and Reynolds-Averaged Navier-Stokes (RANS) equations, which can consider viscous flow effects, are used for the aerodynamic calculations. Three iterations are performed based on a result of a convergence study with the cost-efficient medium-fidelity analysis. Figure 6 shows the result of the convergence study.

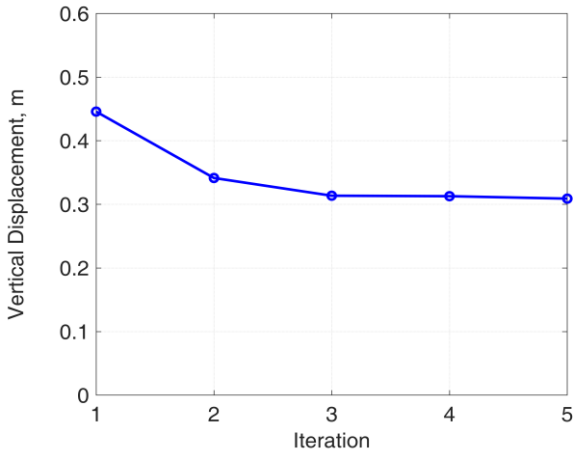

Figure 6: Wing tip vertical deflection with different iterations obtained by the medium-fidelity framework.

The vertical wing deflections along the mid-chord obtained by three different aerodynamic solvers are shown in Fig. 7. Note that the flexible wings experience large vertical deflections more than 30% of semi-span. Figure 8 shows the 3-D wing deformations at each iteration obtained by the CFD with the RANS equations, which can easily confirm the large deflection. Therefore, it is important to perform geometrically nonlinear analysis to obtain accurate solutions for such highly flexible wings [18]. In addition, at low Mach number, the solution by the CFD with the Euler equations shows a reasonable agreement with the solution using the UVLM for the aerodynamic solver (i.e. the error of the wing tip vertical deflection to the solution with the UVLM is 3.49%). On the other hand, the solution by the CFD with the

RANS equations gives the larger deflection (i.e. the error to the solution with the UVLM is 16.63%). Two reasons for the large difference can be considered. The first reason of the difference is the existence of the aerodynamic loads due to the friction in the solution by the CFD with the RANS equations. The second reason is that the lift is increased because the effective wing thickness is increased due to the displacement thickness caused by the effect of viscous flow as shown in Fig. 9. The comparison of computational times for the aeroelastic simulations with different aerodynamic solvers is listed in Table 1. The simulations were mainly performed on a computer with 2.5 GHz Intel Core i7-7660U CPU and 16 GB RAM. The CFD calculations were performed on the JAXA Supercomputer System generation 2 (JSS2) using 160 threads. The transformations of aerodynamic solutions obtained by the CFD to the structural model were performed on a computer with 3.3 GHz Intel Core i9-9940X CPU and 64 GB RAM due to the computational resources. By comparing with the aeroelastic simulation using the UVLM, it is found that the simulations using the CFD with the Euler and RANS equations require more than 100 times longer computations. For problems as the present cases, since the medium-fidelity aeroelastic analysis with the UVLM can provide a close result to the high-fidelity aeroelastic with the Euler-based CFD, the medium-fidelity analysis has advantages with respect to computational cost. On the other hand, the high-fidelity analysis with the CFD is required at higher (close to transonic) speed since it is known that the UVLM with the compressible correction loses its accuracy around the flow speed [27]. In addition, to properly evaluate aeroelastic characteristics with effects of viscous flow, it is necessary to perform the high-fidelity analysis using a CFD with a model, which can consider viscous effects, such as the RANS model. Otherwise, a large discrepancy occurs between a numerical solution and an actual wing behavior.

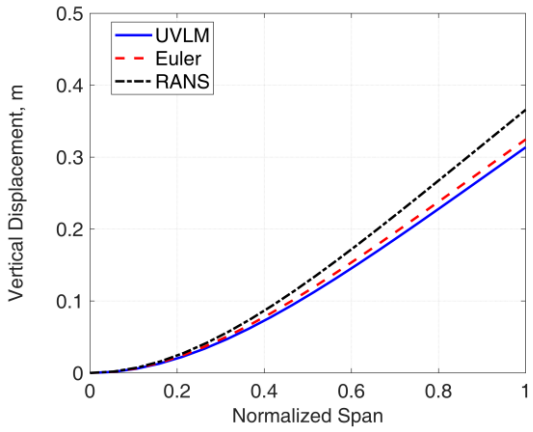

Figure 7: Vertical wing deflections along the mid-chord at the steady-state flight with different aerodynamic solvers.

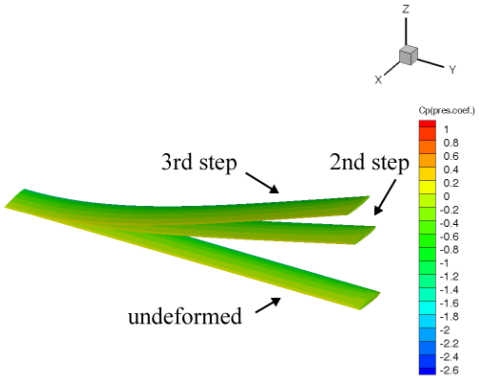

Figure 8: Wing deformations and pressure coefficient distributions at each iteration obtained by the CFD with the RANS equations.

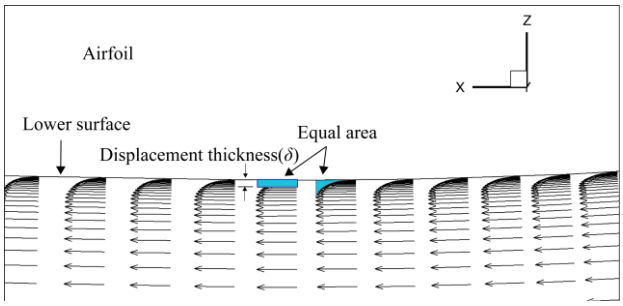

Figure 9: Flow velocity vectors around the lower surface boundary in the vicinity of the position along the chord at which maximum thickness occurs obtained by the CFD with the RANS equations with the displacement thickness image.

Table 1: Comparison of the computational times.

	UVLM	CFD (Euler)	CFD (RANS)
Time, s	286	36335	51914
Ratio to UVLM	1	126.91	181.32

4 CONCLUDING REMARKS

In this paper, the multi-fidelity geometrically nonlinear aeroelastic framework to study nonlinear aeroelastic responses of highly flexible wing have been developed. For the computationally efficient medium-fidelity analysis, which is suitable for preliminary studies, the UVLM formulation was coupled with the geometrically nonlinear structural solver using the corotational shell finite element. For the more accurate high-fidelity analysis, a fast unstructured CFD code developed by JAXA was integrated with the same structural model. Aeroelastic simulations were performed with the different fidelity aeroelastic analysis configurations and the solutions were compared to evaluate in term of accuracies and computational costs.

In the numerical studies, it was confirmed that it was important to consider the geometrical nonlinearity in the analysis of a highly flexible wing because such a wing easily undergoes large deformations. Also, especially in subsonic flight condition, the cost-effective medium-fidelity aeroelastic analysis with the UVLM was clearly beneficial since it could provide a close solution to the CFD-based solution with the Euler equations. However, the more accurate high-fidelity CFD-based analysis with the RANS equations was required for an aeroelastic evaluation with viscous effects. In future works, further verifications of the analysis frameworks with experimental results should be performed. In addition, although the transformation of aerodynamic solutions from the CFD code to the structural model was implemented for and performed on a stand-alone computer, the parallel computing technique will be implemented for an acceleration of the high-fidelity analysis.

5 REFERENCES

[1] Pendleton, E., Flick, P., Paul, D., Voracek, D. F., Reichenbach, E., and Griffin, K. (2007). The X-53 A Summary of the Active Aeroelastic Wing Flight Research Program. *48th AIAA/ASME/ASCE/AHS/ ASC Structures, Structural Dynamics and Materials Conference and Exhibit.* AIAA Paper 2007-1855.

[2] Cumming, S. B., Smith, M. S., Ali, A., Bui, T. T., Ellsworth, J., and Garcia, C. A. (2016). Aerodynamic Flight Test Results for the Adaptive Compliant Trailing Edge. *AIAA Atmospheric Flight Mechanics Conference,* AIAA Paper 2016-3855.

[3] Nguyen, N., Lebofsky, S., Ting, E., Kaul, U., Chaparro, D., and Urnes, J. (2015). Development of Variable Camber Continuous Trailing Edge Flap for Performance Adaptive Aeroelastic Wing. *SAE 2015 AeroTech Congress and Exhibition*, SAE Technical Paper 2015-01-2565.

[4] Burdette, D. A., and Martins, J. R. R. A. (2018). Impact of Morphing Trailing Edges on Mission Performance for the Common Research Model. *Journal of Aircraft,* 56(1), 369-384.

[5] Cooper, J. E., Chekkal, I., Cheung, R. C. M., Wales, C., Allen, N. J., Lawson, S., Peace, A. J., Cook, R., Standen, P., Hancock, S. D., and Carossa, G. M. (2015). Design of a Morphing Wingtip. *Journal of Aircraft,* 52(5), 1394-1403.

[6] Vasista, S., Riemenschneider, J., van de Kamp, B., Monner, H. P., Cheung, R. C. M., Wales, C., and Cooper, J. E. (2016). Evaluation of a Compliant Droop-Nose Morphing Wing Tip via Experimental Tests. *Journal of Aircraft,* 54(2), 519-534.

[7] Tsushima, N., and Su, W. (2016). Concurrent Active Piezoelectric Control and Energy Harvesting of Highly Flexible Multifunctional Wings. *Journal of Aircraft,* 54(2), 724-736.

[8] Tsushima, N., and Su, W. (2017). Flutter suppression for highly flexible wings using passive and active piezoelectric effects. *Aerospace Science and Technology,* 65, 78-89.

[9] Tsushima, N., and Su, W. (2016). Modeling of Highly Flexible Multifunctional Wings for Energy Harvesting. *Journal of Aircraft,* 53(4), 1033-1044.

[10] Ortiz, P., and Alley, N. Spanwise Adaptive Wing-PTERA Flight Test. NASA AFRC-E-DAA-TN57887.

[11] Kantor, E., Raveh, D. E., and Cavallaro, R. (2019). Nonlinear Structural, Nonlinear Aerodynamic Model for Static Aeroelastic Problems. *AIAA Journal,* 57(5), 2158-2170.

[12] Wang, Y., Wynn, A., and Palacios, R. (2018). Nonlinear Aeroelastic Control of Very Flexible Aircraft Using Model Updating. *Journal of Aircraft,* 55(4), 1551-1563.

[13] Jung, Y. S., Yu, D. O., and Kwon, O. J. (2016). Aeroelastic Analysis of High-Aspect-Ratio Wings Using a Coupled CFD-CSD Method. *Transactions of the Japan Society for Aeronautical and Space Sciences,* 59(3), 123-133.

[14] Chimakurthi, S. K., Stanford, B. K., Cesnik, C. E., and Shyy, W. (2009). Flapping wing CFD/CSD aeroelastic formulation based on a corotational shell finite element. *50th AIAA/ASME/ASCE/AHS/ASC Structures, Structural Dynamics, and Materials Conference,* AIAA Paper 2009-2412.

[15] Arizono, H., and Cesnik, C. E. (2013). Computational Static Aeroelasticity Using Nonlinear Structures and Aerodynamics Models. *54th AIAA/ASME/ASCE/AHS/ASC Structures, Structural Dynamics, and Materials Conference,* AIAA Paper 2013-1862

[16] de Souza, C., da Silva, R. G., and Cesnik, C. (2012). Nonlinear aeroelastic framework based on vortex-lattice method and corotational shell finite element. *53rd AIAA/ASME/ASCE/AHS/ASC Structures, Structural Dynamics and Materials Conference,* AIAA Paper 2012-1976.

[17] Su, W., Huang, Y., and Hammerton, J. R. (2017). Nonlinear Aeroelasticity of Highly Flexible Joined-Wing Aircraft using Unsteady Vortex-Lattice Method. *58th AIAA/ASCE/AHS/ASC Structures, Structural Dynamics, and Materials Conference,* AIAA Paper 2017-1353.

[18] Tsushima, N., Yokozeki, T., Su, W., and Arizono, H. (2019). Geometrically nonlinear static aeroelastic analysis of composite morphing wing with corrugated structures. *Aerospace Science and Technology,* 88, 244-257.

[19] Tsushima, N., Arizono, H., Yokozeki, T., and Su, W. (2019). Nonlinear aeroelasticity of morphing wings with corrugated structures. *60th AIAA/ASCE/AHS/ASC Structures, Structural Dynamics, and Materials Conference*. AIAA Paper 2019-0219.

[20] Felippa, C. A. (2003). A study of optimal membrane triangles with drilling freedoms. *Computer Methods in Applied Mechanics and Engineering,* 192(16-18), 2125-2168.

[21] Batoz, J. L., Bathe, K. J., and Ho, L. W. (1980). A study of three-node triangular plate bending elements. *International Journal for Numerical Methods in Engineering,* 15(12), 1771-1812.

[22] Khosravi, P., Ganesan, R., and Sedaghati, R. (2007). Corotational non-linear analysis of thin plates and shells using a new shell element. *International Journal for Numerical Methods in Engineering,* 69(4), 859-885.

[23] Shearer, C., and Cesnik, C. (2006). Modified generalized alpha method for integrating governing equations of very flexible aircraft. *47th AIAA/ASME/ASCE/AHS/ASC Structures, Structural Dynamics, and Materials Conference,* AIAA Paper 2006-1747.

[24] Katz, J., and Plotkin, A. (2001). *Low-speed aerodynamics*. Cambridge, UK: Cambridge University Press.

[25] Hashimoto, A., Murakami, K., Aoyama, T., Ishiko, K., Hishida, M., Sakashita, M., and Lahur, P. (2012). Toward the Fastest Unstructured CFD Code 'FaSTAR'. *50th AIAA Aerospace Sciences Meeting including the New Horizons Forum and Aerospace Exposition*. AIAA Paper 2012-1075.

[26] Ito, Y., Murayama, M., Yamamoto, K., Shih, A. M., and Soni, B. K. (2013). Efficient Hybrid Surface/Volume Mesh Generation Using Suppressed Marching-Direction Method. *AIAA Journal,* 51(6), 1450-1461.

[27] Melin, T., Isikveren, A. T., and Friswell, M. I. (2010). Induced-Drag Compressibility Correction for Three-Dimensional Vortex-Lattice Methods. *Journal of Aircraft,* 47(4), 1458-1460.

COPYRIGHT STATEMENT